Highly Efficient Yellow Organic Light Emitting Diode with a Novel Wet- and Dry-Process Feasible Iridium Complex Emitter

Jwo-Huei Jou, You-Xing Lin, Shiang-Hau Peng, Chieh-Ju Li, Yu-Min Yang, Chih-Lung Chin, Jing-Jong Shyue, Shih-Sheng Sun, Mandy Lee, Chien-Tien Chen, Ming-Chung Liu, Cheng-Chang Chen, Guan-Yu Chen, Jin-Han Wu, Cheng-Hung Li, Chao-Feng Sung, Mei-Ju Lee, and Je-Ping Hu*

Yellow emission is crucial in RGBY display technology and in fabricating physiologically friendly, low color-temperature lighting sources. Emitters with both wet- and dry-process feasibility are highly desirable to fabricate, respectively, high-quality devices via vapor deposition and cost-effective, large-area devices via roll-to-roll fabrication. Here, high-efficiency organic light-emitting diodes with a novel wet- and dry-process feasible yellow-emitting iridium complex, bis[5-methyl-7-fluoro-5H-benzo(c)(1,5) naphthyridin-6-one]iridium (picolinate), are demonstrated. By spin coating, the device shows, at 1000 cd m^{-2}, an external quantum efficiency (EQE) of 18.5% with an efficacy of 52.3 lm W^{-1}, the highest among all reported yellow devices via wet-process, while using vapor deposition, the EQE is 22.6% with a 75.1 lm W^{-1} efficacy, the highest among all dry-processed counterparts. The high efficiency may be attributed to the replacement of the hydrogen atom with a fluorine atom on a 2-substitutional site in the emitter to prevent dense molecular packing-caused self-quenching and to reduce radiationless deactivation rates, leading to a high quantum yield (71%).

1. Introduction

Organic light-emitting diodes (OLEDs) can be used in high quality flat panel displays and lighting applications.[1] Among them, yellow emission is one crucial chromaticity component such as for RGBY-TV, lithography labs, traffic lights, and signal lights etc. Most importantly, it serves as a backbone emission for physiologically-friendly very-low color temperature lighting sources for use at night due to its comparatively low per lumen suppression effect on melatonin secretion.[2] To make the resultant products more energy saving and last longer, yellow OLEDs with higher power efficiency are highly demanded. It would be more ideal if the electroluminescently effective yellow emitters possess both wet- and dry-process feasibility to realize, respectively, cost-effective large area-size roll-to-roll manufacturing and high performance devices.

Over the past years, some efficient yellow OLEDs had been reported.[3,4] Taking the devices via wet-process for examples, Xie's group reported a 20 lm W^{-1} efficacy at 1000 cd m^{-2} for a yellow iridium phosphorescent guest with an electron-withdrawing trifluoromethyl (CF_3) substituent on the ligand doped in a dendritic host.[3a] Xiang's group reported 11 lm W^{-1} by using a platinum based complex with a tetramethylethylene group doped in a molecular host of 4,4′-N,N'-dicarbazole-biphenyl (CBP).[3b]

Prof. J.-H. Jou, Y.-X. Lin, S.-H. Peng, C.-J. Li, Y.-M. Yang
Department of Materials Science and Engineering
National Tsing Hua University
No. 101, Section 2, Kuang-Fu Road, Hsin-Chu, 30013,
Taiwan Republic of China
E-mail: jjou@mx.nthu.edu.tw
Dr. C.-L. Chin
Material and Chemical Research Laboratories
Industrial Technology Research Institute
Hsin-Chu, 30013, Taiwan Republic of China
Dr. J.-J. Shyue
Research Center for Applied Sciences
Academia Sinica
Tai-Pei, 11529, Taiwan Republic of China
Dr. S.-S. Sun, M. Lee
Institute of Chemistry
Academia Sinica, Tai-Pei, 11529,
Taiwan Republic of China
Prof. C.-T. Chen
Department of Chemistry
National Tsing Hua University
Hsin-Chu, 30013, Taiwan Republic of China
Dr. M.-C. Liu, Dr. C.-C. Chen, Dr. G.-Y. Chen,
J.-H. Wu, C.-H. Li
Advance Lighting Technology Department
Industrial Technology Research Institute
Hsin-Chu, 31040, Taiwan Republic of China
C.-F. Sung, M.-J. Lee, Dr. J.-P. Hu
Electronics and Optoelectronics Research Laboratories
Industrial Technology Research Institute
Hsin-Chu, 31040, Taiwan Republic of China

DOI: 10.1002/adfm201302013

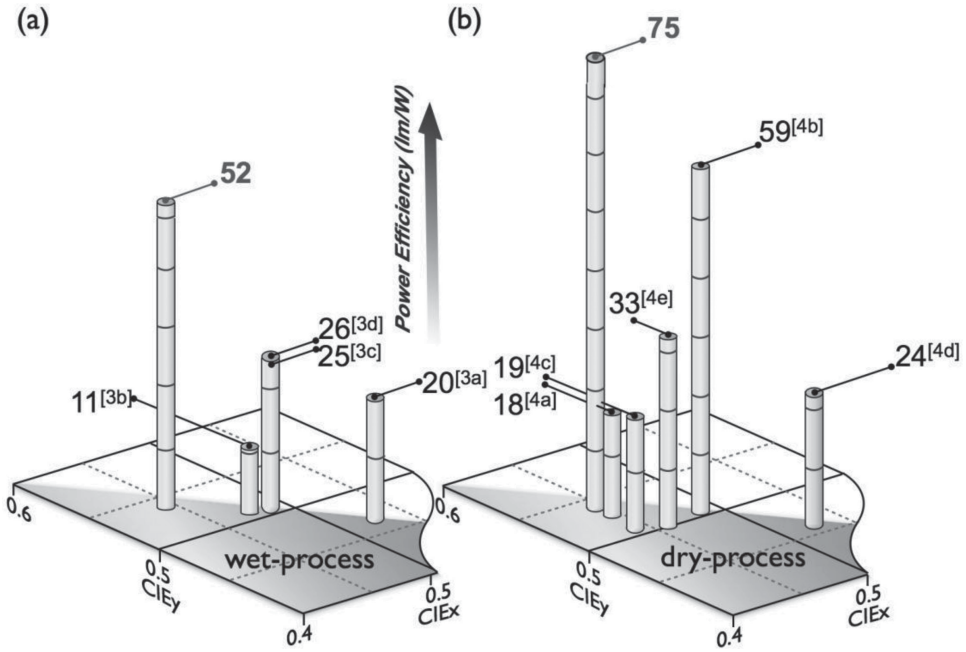

Figure 1. Comparison, on the CIE diagram, of the power efficiency results of the novel yellow 2-FBNO containing OLEDs, fabricated via wet- and dry-processes, against those previously reported. All the efficacy data were taken at 1000 cd m^{-2}.

Jou's group reported 25 lm W^{-1} by using a yellow thiophene containing iridium phosphorescent emitter doped in a molecular host of CBP,[3c] or 26 lm W^{-1} doped in a mixed hosts of 4,4′,4″-tri(*N*-carbazolyl)triphenylamine (TcTa) and bis(3,5-difluoro-2-(2-pyridyl) phenyl-(2-carboxypyridyl)iridium(III) (FIrpic).[3d]

By using thermal evaporation deposition, Jou's group reported an 18 lm W^{-1} efficacy at 1000 cd m^{-2} by using a seven-membered-ring based fluorescent yellow emitter dispersed in a step-wise tri-emissive layered structure.[4a] Jou's group reported 59 lm W^{-1} by using a single thiophene containing iridium based yellow emitter doped in a mixed hosts of 1,3,5-tris(*N*-phenyl-benzimidazol-2-yl) benzene (TPBi) and green emitter tris(2-phenylpyridine) iridium(III) ($Ir(ppy)_3$).[4b] Ma's group reported 19 lm W^{-1} by using an electron-withdrawing CF_3 substituent modified yellow iridium based guest doped in CBP.[4c]

To fabricate a high efficiency OLED, phosphorescent materials are often used because of their ability to fully utilize both singlet and triplet excitons, achieving a nearly 100% internal quantum efficiency.[5] Many researchers had thus put tremendous efforts in designing and synthesizing high efficiency phosphorescent materials.[6] From molecular design perspective, using different types of cyclometalated ligands or introducing special functional groups to the ligands can modify the electroluminescence and processing characters of the phosphorescent complexes.[7] Taking fluorination for examples,[8] using fluorine or CF_3 to replace hydrogen in the cyclometalated ligand could markedly reduce concentration quenching of luminescence and meanwhile increase volatility to favor vapor deposition. Fluorination can also be used to alter the energy levels of emitters, i.e., the highest occupied molecular orbital (HOMO) and the lowest unoccupied molecular orbital (LUMO), which may in turn allow the tuning of color. Sometimes, fluorination can enhance electron mobility, leading to a more balanced carrier injection and hence a higher device efficiency.

We demonstrate in this report the employment of fluorination to markedly improve the device efficiency and processability of an iridium complex based yellow OLED. By using fluorine to replace the 2-substitutional hydrogen in the cyclometalated ligand of the complex of bis[5-methyl-5H-benzo[c][1,5] naphthyridin-6-one]iridium (picolinate) (BNO), the resultant dry-processed 2-FBNO containing device shows, at 1,000 cd m^{-2} for example, an external quantum efficiency (EQE) of 23.5%, while 19.6% the BNO counterpart. If via wet-process, the EQE is 18.5% for the 2-FBNO containing device, while 13.6% for the BNO counterpart. In addition, the power efficiency for the 2-FBNO containing device is 75.1 lm W^{-1} via evaporation deposition, the highest among all reported dry-processed yellow OLEDs, or 52.3 lm W^{-1} via spin-coating, the highest among all wet-processed counterparts (**Figure 1**).

2. Results and Discussion

2.1. Synthesis

Scheme 1 shows the synthesis of the pure yellow light-emitting guest 2-FBNO. Iridium(III) trichloride hydrate was first reacted with 5-methyl-7-fluoro-5H-benzo[c][1,5]naphthyridin-6-one to give the corresponding cyclometalated iridium(III)-μ-chloro-bridged dimers. Further reaction of the dimers with picolinic acid and sodium carbonate formed the desired iridium complex, 2-FBNO. The description regarding how the ligand, 5-methyl-7-fluoro-5H-benzo[c][1,5] naphthyridin-6-one, is synthesized can be referred to in the literature.[9]

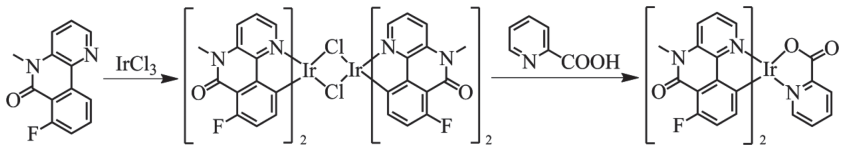

Scheme 1. Schematic illustration of the synthesis of the novel yellow dopant, 2-FBNO.

2.2. Thermal Properties

The 2-FBNO molecule exhibits a decomposition temperature at 425 °C, determined by thermal-gravimetric analysis (**Table 1**). As to the comparing counterpart, BNO, it also shows a high decomposition temperature of 402 °C. The high decomposition temperature would prevent either molecule from degradation during thermal evaporation deposition, and hence enable them to be dry-processable.

No measurable glass transition was found for all these two emitters, 2-FBNO and BNO at temperatures before reaching their decomposition temperatures. However, the highly conjugated polycyclic structure should ensure these two molecules to be solution-processable due to their incredibly high thermal stability that can prevent film integrity deteriorating owing to vigorous solvent vaporization upon drying.

2.3. Photophysical Properties

Figure 2 shows the ultraviolet-visible (UV-Vis) and photoluminescence (PL) spectra of 2-FBNO and BNO dissolved in dichloromethane (CH_2Cl_2) at room temperature. As comparing with those of BNO, the UV absorption bands of 2-FBNO show bathochromic shift at wavelengths below 360 nm that correspond to its ligand-centered π–π^* transitions, and at wavelengths between 380 and 500 nm that correspond to its metal-to-ligand charge transfer (^{1}MLCT and ^{3}MLCT). Upon excitation, the corresponding PL emission of 2-FBNO peaks at 545 nm, a bathochromic shift of 30 nm from the peak emission of 515 nm for BNO.

The quantum yields are 71% and 46%, respectively, for the yellow emitter 2-FBNO and green emitter BNO dissolved in degassed CH_2Cl_2 at room temperature, and which are calibrated by using the well-known green emitter $Ir(ppy)_3$ as a standard, whose quantum yield is 40%.[10] Their corresponding excited-state lifetimes are 3.72 and 2.47 μs, respectively.

The comparatively higher quantum yield of the yellow 2-FBNO emitter should warrant its resulting device a higher efficiency. The reason for the higher quantum yield may be attributed to the fact that replacing the H- with F-atom can lower the molecular vibrations, and consequently reduce the rate of radiationless deactivation. This can be evidenced by the resultant lower non-radiative rate constant, k_{nr}, i.e. 0.78×10^5 s^{-1}, which is nearly two times lower than the BNO counterpart, i.e. 2.19×10^5 s^{-1}. Whilst, the two molecules have nearly the same radiative rate constant, k_r, it is 1.91×10^5 s^{-1} for 2-FBNO and 1.86×10^5 s^{-1} for BNO. The lesser radiationless deactivation coupling with a nearly unchanged radiative relaxation has hence resulted in a higher quantum yield for the 2-FBNO as observed.

According to the quantum chemical calculations using the density functional theory (DFT), the 2-substitutional site of BNO molecule is localized more at the vicinity of the HOMO, as illustrated in **Figure 3**. When the F-atom is introduced at the 2-substitutional site, the resulting LUMO is decreased from –1.93 to –2.10 eV, a decrement of 0.17 eV, while the HOMO is slightly increased from –5.39 to –5.35 eV, an increment of 0.04 eV. The decrease in the LUMO energy level may be attributed to the stabilization effect on the LUMO of the 2-FBNO molecule from the electron-withdrawing character of the F-atom.

The reason why the HOMO is increased only slightly may be attributed to two effects that counterbalance each other. The first is resulted from the same stabilization effect from the electron-withdrawing F-atom on the HOMO of the 2-FBNO molecule, leading to a lower HOMO energy level. Whilst, the second is resulted from a direct repelling interaction between the 2p-orbital of the F-atom and the HOMO of the 2-FBNO molecule, which would destabilize the HOMO and hence increase the HOMO energy level.

These explain why the 2-FBNO molecule shows a significantly smaller band gap, which is 3.25 eV, while 3.46 eV for BNO. These also explain why the emission red-shifts from green to yellow as the F-atom is introduced to replace the H-atom in the 2-substitutional site. The trends shown in the above simulation results match with those found experimentally. Specifically, the difference in band gap between 2-FBNO and BNO is 0.21 eV from simulation, while 0.15 eV from experiment.

Table 1. Electrochemical, photophysical, and thermal characteristics of the novel yellow emitter 2-FBNO and the comparing green emitter BNO.

Compound	HOMO[a] [eV]	LUMO[a] [eV]	Band gap [eV]	Φ_p[b] [%]	τ[c] [μs]	k_r [10^5 s^{-1}]	k_{nr} [10^5 s^{-1}]	T_d[d] [°C]
2-FBNO	5.57(5.35)	3.18(2.10)	2.39(3.25)	71	3.72	1.91	0.78	425
BNO	5.59(5.39)	3.05(1.93)	2.54(3.46)	46	2.47	1.86	2.19	402

[a]HOMO and LUMO values are measured by the cyclic voltammetry (CV) method. The semi-oxidation potential ($E_{1/2}^{ox}$) could be calculated from (E_{p1}+E_{p2})/2–0.48. 0.48 is the correction value obtained by the oxidation system was added Ferrocenium/Ferrocene (Fc^+/Fc) as the internal standard, and then the energy of HOMO could be obtained from the $E_{HOMO} = -(E_{1/2}^{ox} + 4.8)$. The semi-reduction potential ($E_{1/2}^{red}$) could be calculated from (E_{p1}+E_{p2})/2–0.48, and then the energy of LUMO could be obtained from the $E_{LUMO} = -(E_{1/2}^{red} + 4.8)$. The data in parentheses are obtained by DFT calculations; [b]Quantum yield measured in CH_2Cl_2 at room temperature; [c]Excited-stated lifetime measured in CH_2Cl_2 at room temperature; [d]Decomposition temperature.

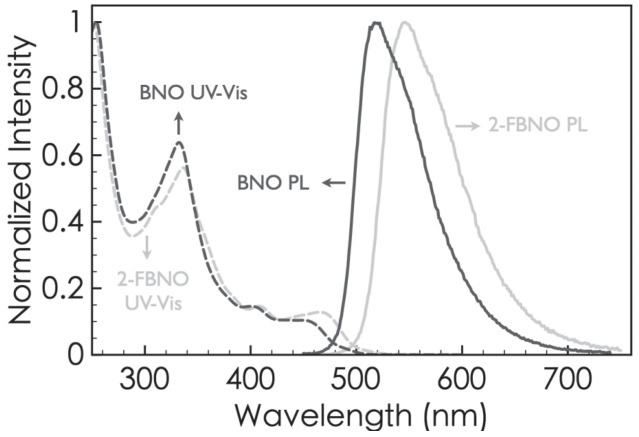

Figure 2. Comparison of the ultraviolet-visible and photoluminescence spectra of the innovative yellow 2-FBNO emitter with those of the green BNO emitter. The data were measured in CH_2Cl_2 at room temperature.

2.4. Wet-Processed OLED Devices

Figure 4 shows all the studied OLEDs device structure and their corresponding energy level diagrams. The device is composed of a 125 nm indium tin oxide (ITO) anode layer, following (a) a 35 nm poly(3,4-ethylene-dioxythiophene)-poly(styrenesulfonate) (PEDOT:PSS) hole-injection layer (HIL), a 20 nm single emissive layer (EML) via spin-coating for wet-process, while (b) a 2.5 nm 1,4,5,8,9,11-hexaazatriphenylene-hexacarbonitrile (HAT-CN) charge generation layer (GCL), a 35 nm di-[4-(*N,N*-ditolylamino)-phenyl]cyclohexane (TAPC) hole transporting layer (HTL), a 20 nm single EML via evaporation deposition for dry-process, then a 45 nm 1,3-bis(3,5-dipyrid-3-yl-phenyl)benzene (BmPyPB) electron-transporting layer (ETL), a 1 nm lithium fluoride (LiF) layer, and a 100 nm aluminum (Al) cathode layer.

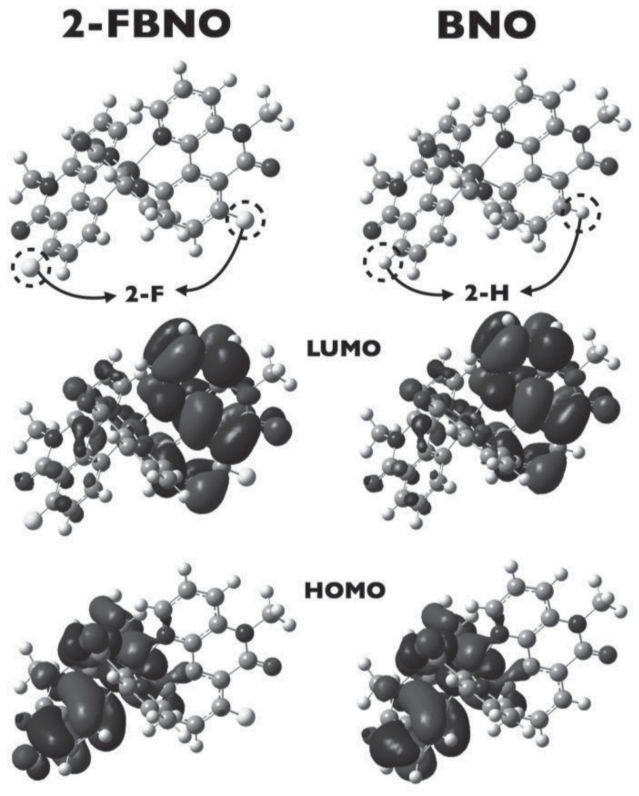

Figure 3. Effect of F-atom substitutional site on the electron distributions of the two BNO-based emitters, i.e. the present yellow emitter of 2-FBNO and the comparing green emitter of BNO, calculated according to the density functional theory.

The effect of the doping concentration of 2-FBNO on device efficiency is summarized in **Table 2**. Taking 1000 cd m^{-2} for example, the power efficiency is slightly increased from 50.3 to 52.3 lm W^{-1} as the doping concentration is increased from 20 wt% to 25 wt%. As the concentration is increased to 30 wt%, the power efficiency starts to drop, which may be attributed to triplet-triplet annihilation as well as concentration-quenching, resulted from self-aggregation of the emitter at high concentration. At the optimized doping concentration, i.e., 25 wt%, no blue emission from the host is observable in the resultant EL spectrum, shown in **Figure 5**(a), indicating a complete host-to-guest energy transfer to have occurred.

The film morphology and device efficiency of the two emitters, yellow 2-FBNO and green BNO, are compared on basis of the same spin-coating process at the same 25 wt% concentration doped in the host of TcTa. The respective surface roughness is 0.58 nm for the 2-FBNO composing film, which is extremely similar to the 0.59 nm for the BNO composing counterpart, as shown by their atomic-force microscope (AFM) images in **Figure 6**. The relatively good film integrity should consequently warrant these two emitters containing devices a sound feasibility in device fabrication using wet-process.

Indeed, both emitters show relatively good efficiency performance via the aforementioned spin-coating. Moreover, the efficiency shown by the 2-FBNO containing device is better than the BNO containing counterpart as shown in Figure 6(b). At 1000 cd m^{-2}, for example, the EQE is 18.5% with a 52.3 lm W^{-1} efficacy for the yellow 2-FBNO containing device, while 13.6% with a 38.9 lm W^{-1} for the green BNO counterpart. Besides its high quantum yield, the reason why the yellow 2-FBNO containing device shows a better device efficiency may be attributed to the F-substituent that exhibits good electron affinity. Especially, hole is the major carrier in such a device structure because the host TcTa is an excellent hole-conductive material.[11] To balance the injection of electron against that of hole, the electron affining 2-FBNO seemly is more effective in attracting electrons, hence leading to a more balanced carrier injection and likewise a higher device efficiency as observed.

To demonstrate if the new yellow emitter, 2-FBNO, is truly efficient as fabricated via wet-process, its efficacy and EQE results measured at 1000 cd cm^{-2}, for example, are compared against those of the previous efficiency record holding yellow emitter, bis(4-phenylthieno[3,2-c]pyridinato-N,C 2')acetylacetonate iridium(III) (PO-01).[3d] Based on the same device structure and wet-process using optimized doping concentration, the PO-01 containing device exhibits an efficacy of 34.2 lm W^{-1} and an EQE of 14.7% EQE, both which are significantly lower than the 52.3 lm W^{-1} and 18.5% EQE for the 2-FBNO containing

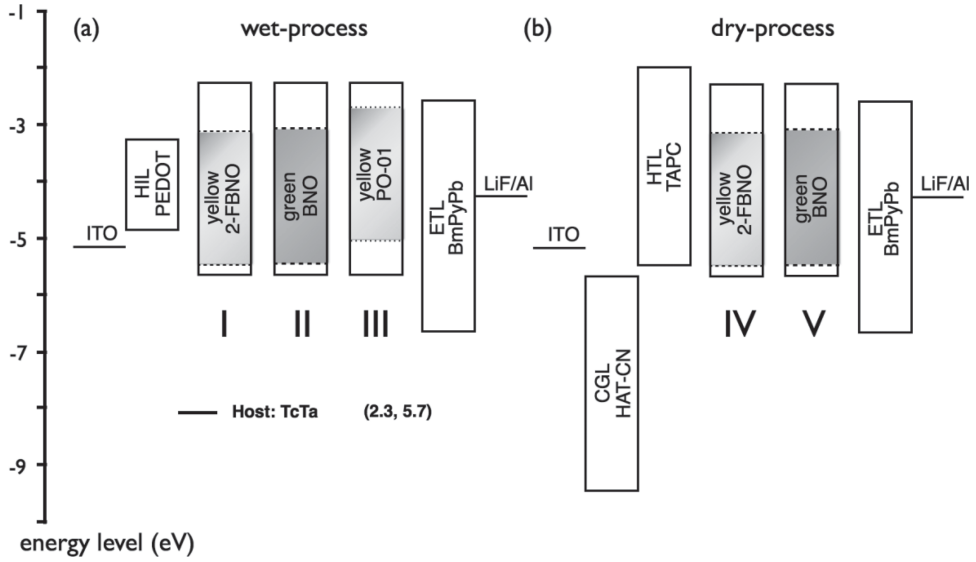

Figure 4. Schematic diagrams of the energy-levels of the OLED devices containing the presented yellow light-emitting 2-FBNO, comparing with those containing the green BNO and yellow PO-01 emitters, via (a) wet-process and (b) dry-process.

counterpart. These results confirm 2-FBNO to be a highly electroluminescence-active yellow emitter.

2.5. Dry-Processed OLED Devices

The efficiency performance of the yellow light-emitting 2-FBNO is further investigated via vapor evaporation deposition. The resultant efficiency of the 2-FBNO containing device is also better than the BNO containing counterpart, as shown in **Figure 7**(a). At 1000 cd m^{-2}, for example, the 2-FBNO containing device shows an EQE of 23.5% with a 58.9 lm W^{-1} efficacy, higher the 19.6% with a 48.3 lm W^{-1} for the green BNO counterpart. In these dry-processed devices, a HTL that possesses a 0.3 eV electron confining barrier is incorporated between the ITO and EML. The resultant effective electron confinement has hence led to a much lesser efficiency roll-off at elevated voltages, especially as comparing with that observed in the wet-processed device, in which excessively injected electrons at elevated bias could not be retained in the EML due to the lack of any electron confining barrier. It is believed that the efficiency of the device fabricated via wet-process can be further improved at high bias, provided an effective electron-confining-function possessing hole transporting material with wet-process feasibility is devised and inserted between the HIL, PEDOT:PSS, and the EML.[12]

To further improve the efficacy of the 2-FBNO containing yellow device, a CGL (HAT-CN), is deposited on top of the ITO anode to enhance hole injection. As shown in Figure 7(b), the resultant current density and luminance are, indeed, markedly

Table 2. Effects of different doping concentrations, emitters, and process methods on the power efficiency (PE), external quantum efficiency (EQE), current efficiency (CE), and CIE coordinates of the novel yellow emitter, 2-FBNO, containing OLED devices, comparing with those of the counterparts with the green emitter, BNO, and the efficient yellow emitter, PO-01.

	Device	Dopant	Conc. [wt%]	Operation Voltage [V]	PE [lm W^{-1}]	CE [cd A^{-1}]	EQE [%]	1931 CIE Coordinates	Maximum Luminance [cd m^{-2}]
					At 100/1000/10 000 cd m^{-2}				
W[a)]	I-1	2-FBNO	15	3.1/3.8/5.1	62.5/51.1/25.2	61.8/61.4/40.4	17.1/16.9/11.1	(0.43,0.56)/(0.43,0.56)/(0.43,0.56)	21,340
	I-2		20	3.2/3.9/5.2	61.1/50.3/26.0	65.2/62.5/42.6	18.4/17.8/11.9	(0.44,0.55)/(0.44,0.55)/(0.44,0.55)	23,420
	I-3		25	3.2/3.9/5.2	64.4/52.3/26.1	65.7/64.7/42.9	18.9/18.5/12.2	(0.45,0.54)/(0.45,0.54)/(0.45,0.54)	23,900
	I-4		30	3.5/4.1/5.7	56.7/47.2/20.3	63.2/62.1/36.5	18.3/18.0/10.5	(0.45,0.54)/(0.45,0.54)/(0.45,0.54)	23,000
	II	BNO	25	3.4/4.1/5.3	47.1/38.9/22.7	50.9/50.5/38.2	13.7/13.6/10.3	(0.35,0.61)/(0.35,0.61)/(0.34,0.61)	26,870
	III	PO-01	15	3.4/4.1/5.2	40.1/34.2/23.0	45.2/44.1/37.7	15.1/14.7/12.3	(0.50,0.49)/(0.50,0.49)/(0.50,0.49)	40,700
D[b)]	IV	2-FBNO	25	3.3/4.3/6.2	75.2/58.9/33.3	80.0/81.2/65.0	23.4/23.5/18.8	(0.45,0.54)/(0.45,0.54)/(0.45,0.54)	45,470
	IV*	2-FBNO	25	2.8/3.3/5.3	84.8/75.1/36.6	75.9/77.9/61.0	22.1/22.6/17.6	(0.45,0.54)/(0.45,0.54)/(0.45,0.54)	41,200
	V	BNO	25	3.6/4.7/6.5	60.6/48.3/31.3	69.5/72.6/64.9	18.9/19.6/17.5	(0.36,0.61)/(0.35,0.61)/(0.35,0.61)	54,980

[a)]Wet-process; [b)]Dry-process. The device marked with "*" is incorporated with HAT-CN.

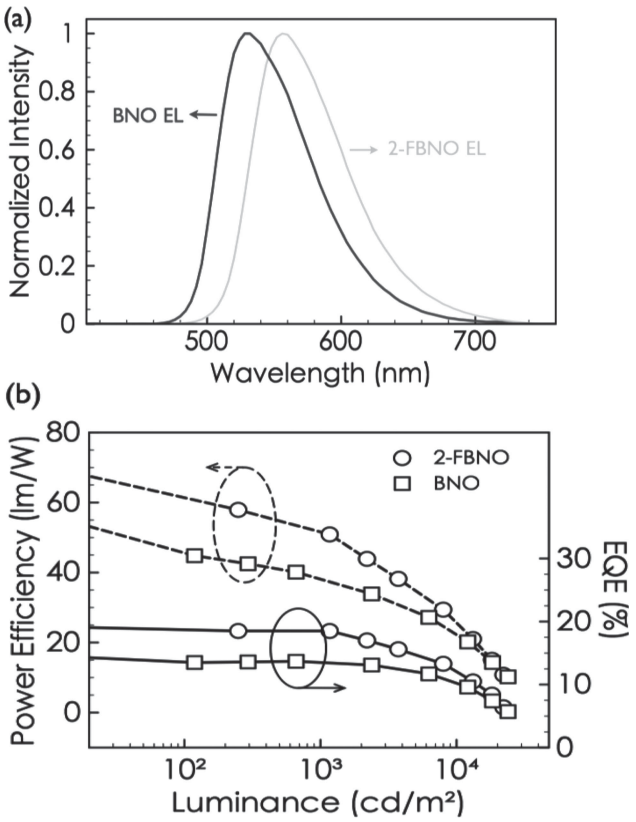

Figure 5. (a) The resulting 2-FBNO also shows a red-shift in electroluminescent spectrum as comparing with that of the green BNO counterpart. (b) Marked improvement in the efficacy and external quantum efficiency of the solution-processed device upon modifying the containing green emitter, BNO, with a fluorine atom in the 2-substitutional site.

increased as a 2.5 nm HAT-CN is incorporated, confirming HAT-CN to be a highly effective hole-injection material as revealed in the literature.[13] The corresponding operation voltage required has hence become lower and the obtained efficacy higher. At 1000 cd m^{-2}, for example, the operational voltage is decreased from 4.3 to 3.3 V, and the efficacy is increased from 58.9 lm W^{-1} to 75.1 lm W^{-1}, with an EQE of 22.6%. In addition, efficacy roll-off has been much improved, and the device still shows comparatively high efficacy and high EQE at elevated luminance; e.g. the efficacy is 49.5 lm W^{-1} with a 20.5% EQE at 5000 cd m^{-2}.

2.6. Comparison with the F and CF_3 Substitution Group

According to a prior study, blue-shift is observed as a CF_3 functional group is introduced into the 2-substitutional site of the BNO molecule.[14] In contrary, red shift is observed as the functional group is replaced by an F-atom. Based on the density functional theory, the HOMO of BNO molecule is localized more at the vicinity of the 2-substitutional site. Overall speaking, the HOMO of the BNO molecule would be stabilized more than LUMO upon introducing the electron-withdrawing CF_3 group at the 2-substitutional site. The resulting HOMO is decreased from –5.39 to –5.79 eV, which is lowered more significantly than the LUMO, that is –1.93 to –2.27 eV. As a result, a higher band gap is formed in the 2-CF_3BNO molecule, leading which to show a bluish green emission, while the 2-FBNO shows a yellow counterpart for having a comparatively lower band gap.

It is also observed that the efficiency of the 2-CF_3BNO containing device is comparatively low if fabricated via vapor deposition, although higher vacuum may lead to a better result. Specifically, its efficacy is 21.1 lm W^{-1} and 9.4% EQE at 100 cd m^{-2}, if fabricated at 2×10^{-5} Torr, as previously reported,[14] and 48.4 lm/W and 17.6% EQE at 5×10^{-6} Torr in the present study (Figure S1 and Table S1, Supporting Information). Whilst, its wet-processed shows 70.1 lm W^{-1} and 23.5% EQE. Regardless, the efficiency performance of the dry-processed 2-CF_3BNO containing bluish green device is much poorer than that of the 2-FBNO or BNO counterpart, due to

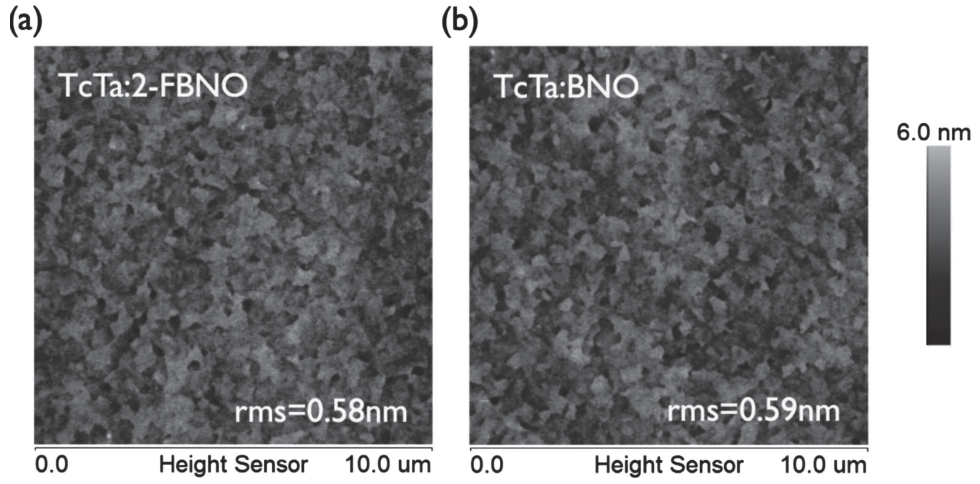

Figure 6. Surface morphologies of the solution-processed films, composing a TcTa host material doped with 25 wt% of (a) the studied yellow 2-FBNO emitter, and (b) the comparing green BNO emitter, by using atomic force microscopy. Both films show nearly the same surface roughness and exhibit good film-forming property during device fabrication.

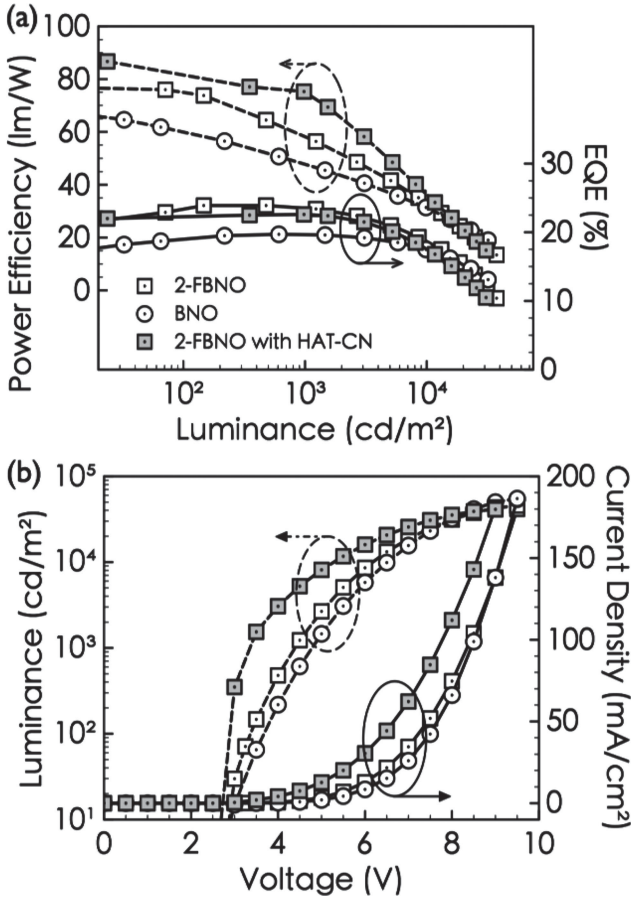

Figure 7. Marked improvement in the (a) efficacy and external quantum efficiency and (b) luminance and current density of the dry-processed device upon modifying the containing green emitter, BNO, with a fluorine atom in the 2-substitutional site. Device performance of the yellow 2-FBNO containing device can be further improved as a charge generation layer, HAT-CN, is incorporated.

its relatively high molecular weight that makes vapor deposition hard to take place. Taking 1000 cd m^{-2} for example, the 2-CF_3BNO containing device exhibits an efficacy of 36.2 lm W^{-1} and an EQE of 16.5%, which are significantly lower than the 58.9 lm W^{-1} and 23.5% EQE for the 2-FBNO containing counterpart, or even lower than the 48.3 W^{-1} and 19.6% EQE for BNO containing counterpart.

3. Conclusion

To conclude, we demonstrate in this report the employment of fluorination in the synthesis of a yellow emitter, 2-FBNO, with both wet-and dry-process feasibility. By using the highly electroluminescence-active emitter, yellow OLEDs with record breaking device efficiency have been fabricated. The device shows, at 1,000 cd m^{-2} for example, an EQE of 18.5% with 52.3 lm W^{-1} by using spin-coating, while 22.6% EQE with 75.1 lm W^{-1} using vapor-deposition. The high efficiency should enable the yellow emitter to serve as a promising candidate in fabricating high quality RGBY displays, or physiologically friendly lighting panels with a very-low color temperature, with a highly energy-saving character via either dry- or wet-process.

4. Experimental Section

Material Characteristic Measurements: Emission spectra were recorded in a degassed solution using a Fluorolog III photoluminescence spectrometer. Samples were degassed via a freeze-thaw-pump cycle at least five times prior to measurements. Luminescence quantum yields were calculated relative to $Ir(ppy)_3$ in CH_2Cl_2 (Φ_{em} = 0.4). Corrected emission spectra were used for the quantum yield measurements. Excited-state lifetimes were measured with a FLSP920 combined time-resolved and steady-state fluorescence Spectrometer. Samples were excited using a microsecond flash lamp as the excitation source. Nonlinear least-squares fitting of the decay curves were performed with the Levenburg-Marquardt algorithm and implemented with the Edinburgh Instruments F900 software. Thermogravimetric analysis (TGA) and was performed under a continuous nitrogen flow using a TA Instruments Q50 at a heating rate of 10 °C min^{-1}. Cyclic Voltammetry experiments were carried out with 1.0 mM of one substrate in a given anhydrous, degassed solvent containing 0.1 M tetrabutylammonium perchlorate (*n*-Bu4NClO4) as a supporting electrolyte on a Chinstruments CH1604A potentiostat. A platinum electrode was used as a counter electrode, and a carbon electrode was used as a working electrode. Ag/AgCl was used as a reference electrode. ^{1}H NMR and ^{13}C spectra were recorded on Mercury-400 (400 MHz 1H, 100 MHz ^{13}C) spectrometers in deuterochloroform with chloroform as an internal reference unless otherwise stated. Chemical shifts are reported in ppm (δ). Coupling constants, *J*, are reported in Hz. MALDI-TOF mass spectra were recorded on an Autoflex III smartbeam LRF200-CID spectrometer. Single crystal X-ray diffraction data were measured using (Mo-K_α) radiation (λ = 0.71073 Å) on a Bruker SMART Apex CCD diffractometer.

Spectral Data of 2-FBNO: MALDI-TOF-MS (m/z): 792 [M + Na]+. ^{1}H NMR (400 MHz, $CDCl_3$, δ): 8.66 (d, *J* = 5.4 Hz, 1H), 8.35 (d, *J* = 7.6 Hz, 1H),7.95 (t, *J* = 7.7 Hz, 1H), 7.79 (d, *J* = 4.7 Hz, 1H), 7.64 (d, *J* = 8.5 Hz, 2H), 7.46 (dd, *J* = 8.5 Hz, 1H), 7.40 (t, *J* = 6.5 Hz,1H), 7.33 (d, *J* = 5.5 Hz, 1H), 7.24 (d, *J* = 5.6 Hz, 1H), 6.87 (m, 2H), 6.57 (dd, *J* = 4.4 Hz,1H), 6.35 (dd, *J* = 4.5 Hz,1H), 3.76(s, 6H). ^{13}C NMR (100 MHz, $CDCl_3$, δ): 172.9, 162.1, 162.0, 152.1, 151.6, 150.2, 148.8, 144.3, 144.0, 143.8, 142.5, 142.1, 141.3, 138.1, 135.6, 135.5, 135.4, 134.3, 133.8, 130.9, 130.5, 128.4, 128.2, 127.1, 126.7, 123.1, 122.9, 122.0, 120.4, 119.8, 29.6, 29.5.

Selected Crystal Data of 2-FBNO: $C_{32}H_{20}F_2IrN_5O_4$; M = 768.73; Triclinic; space group = P -1, a = 13.1543(12) Å, b = 13.9073(13) Å, c = 18.3839(17) Å, V = 3146.0(5) Å^3; Z = 4; ρ_{calcd} = 1.623 Mgm^{-3}; T = 100(2) K; Mo-K_α radiation (λ = 0.71073 Å); μ = 4.299 mm^{-1}; F (000) = 1496; Crystal size = 0.20 × 0.05 × 0.02 mm^3; Reflections collected = 44835, independent reflections = 12742 [R(int) = 0.0355], data/restraints/parameters = 12742/0/797; GOF = 1.175, R_1 (I>2s(I)) = 0.0434, wR_2 (all data) = 0.1184.

Spectral Data of BNO: MALDI-TOF-MS (m/z): 756 [M + Na]+. ^{1}H NMR (400 MHz, $CDCl_3$, δ): 8.68 (d, *J* = 5.6 Hz, 1H), 8.35 (d, *J* = 7.6 Hz, 1H), 7.93 (t, *J* = 7.8 Hz, 2H), 7.87 (d, *J* = 7.8 Hz, 2H), 7.81 (t, *J* = 7.8 Hz, 2H), 7.67 (d, *J* = 8.8 Hz, 2H), 7.45 (dd, *J* = 8.4 Hz, 2H), 7.09 (m, 2H), 6.66 (d, *J* = 7.4 Hz, 1H), 6.46 (d, *J* = 7.4 Hz, 1H), 3.81 (s, 6H). ^{13}C NMR (100 MHz, $CDCl_3$, δ): 172.9, 159.4, 159.1, 158.9, 156.8, 156.3, 152.0, 148.8, 144.3, 142.6, 141.5, 138.4, 138.2, 136.3, 136.1, 135.8, 134.8, 134.3, 128.8, 128.6, 128.4, 123.8, 123.6, 122.2, 118.3, 118.1, 117.9, 117.7, 115.6, 115.2, 29.4, 29.3.

Selected Crystal Data of BNO: $C_{33}H_{24}Cl_2IrN_5O_4$; M = 817.67; Monoclinic; space group = P 1 21/c 1, a = 8.7033(3) Å, b = 21.3151(8) Å, c = 15.3830(6) Å, V = 2802.24(18) Å^3; Z = 4; ρ_{calcd} = 1.938 Mgm^{-3}; T = 100(2) K; Mo-K_α radiation (λ = 0.71073 Å); μ = 5.007 mm^{-1}; F (000) = 1600; Crystal size = 0.30 × 0.17 × 0.06 mm^3; Reflections collected = 30502, independent reflections = 5755 [R(int) = 0.0318], data/restraints/parameters = 5755/0/408; GOF = 1.036, R_1 (I>2s(I)) = 0.0200, wR_2 (all data) = 0.0451.

CCDC 943930 (2-FBNO) and 943929 (BNO) contains the supplementary crystallographic data for this paper. These data can be obtained free of charge from The Cambridge Crystallographic Data Centre via www.ccdc.cam.ac.uk/data_request/cif.

Device Fabrication and Measurement: For wet-process, the fabrication process included firstly spin-coating an aqueous solution of PEDOT:PSS at 4000 rpm for 20 s to form a hole-injection layer on a pre-cleaned ITO anode. Before depositing the following emissive layer, the solution was prepared by dissolving the host and guest molecules in tetrahydrofuran at 50 °C for 0.5 h with stirring. The resulting solution was then spin-coated at 2500 rpm for 20 s under nitrogen. Followed were the depositions of the electron-transporting layer BmPyPB, the electron injection layer LiF, and the cathode Al, by thermal evaporation less than 5×10^{-6} Torr. For dry-process, all the organic layers, LiF, and Al were deposited by thermal evaporation less than 5×10^{-6} Torr. The luminance, CIE chromatic coordinates, and electroluminescent spectrum of the resultant yellow OLEDs were measured by using Photo Research PR-655 spectrascan. Keithley 2400 electrometer was used to measure the current-voltage (I–V) characteristics. The emission area of the devices was 9 mm^2, and only the luminance in the forward direction was measured.

Supporting Information

Supporting Information is available from the Wiley Online Library or from the author.

Acknowledgements

This work was financially supported by Taiwan National Science Council and Ministry of Economic Affairs through grant numbers MEA 101-EC-17-A-07-S1–181, NSC 101–3113-E-007–001, NSC 100–2119-M-007–011-MY3. We also gratefully acknowledge the cooperation of Dr. Chih-Lung Chin in synthesising and providing the studied emitting materials.

Received: June 12, 2013
Published online: August 5, 2013

[1] a) F. So, J. Kido, P. Burrows, *MRS Bull.* **2008**, *33*, 663; b) B. W. D'Andrade, S. R. Forrest, *Adv. Mater.* **2004**, *16*, 1585; c) M. C. Gather, A. Kohnen, K. Meerholz, *Adv. Mater.* **2011**, *23*, 233.

[2] a) G. C. Brainard, B. A. Richardson, T. S. King, R. J. Reiter, *Brain Res.* **1984**, *294*, 333; b) S. W. Lockley, G. C. Brainard, C. A. Czeisler, *J. Clin. Endocr. Metab.* **2003**, *88*, 4502; c) S. M. Pauley, *Med. Hypotheses* **2004**, *63*, 588.

[3] a) B. H. Zhang, G. P. Tan, C. S. Lam, B. Yao, C. L. Ho, L. H. Liu, Z. Y. Xie, W. Y. Wong, J. Q. Ding, L. X. Wang, *Adv. Mater.* **2012**, *24*, 1873; b) H. F. Xiang, S. C. Chan, C. M. Che, P. T. Lai, P. C. Chui, *P. Soc. Photo-Opt. Ins.* **2004**, *5519*, 296; c) J. H. Jou, S. H. Peng, C. I. Chiang, Y. L. Chen, Y. X. Lin, Y. C. Jou, C. H. Chen, C. J. Li, W. B. Wang, S. M. Shen, S. Z. Chen, M. K. Wei, Y. S. Sun, H. W. Hung, M. C. Liu, Y. P. Lin, J. Y. Li, C. W. Wang, *J. Mater. Chem. C* **2013**, *1*, 1680; d) J. H. Jou, C. H. Chen, J. R. Tseng, S. H. Peng, P. W. Chen, C. I. Chiang, Y. C. Jou, J. H. Hong, C. C. Wang, C. C. Chen, F. C. Tung, S. H. Chen, Y. S. Wang, C. L. Chin, *J. Mater. Chem. C* **2013**, *1*, 394.

[4] a) J. H. Jou, Y. S. Wang, C. H. Lin, S. M. Shen, P. C. Chen, M. C. Tang, Y. Wei, F. Y. Tsai, C. T. Chen, *J. Mater. Chem.* **2012**, *22*, 25482; b) J. H. Jou, J. R. Tseng, S. H. Peng, Y. C. Jou, C. H. Lin, S. M. Shen, Y. X. Lin, C. Y. Hsieh, M. K. Wei, D. H. Lin, C. C. Wang, C. C. Chen, F. C. Tung, S. H. Chen, Y. S. Wang, *J. Mater. Chem. C* **2013**, DOI: 10.1039/c3tc30818a; c) C. L. Ho, W. Y. Wong, Q. Wang, D. G. Ma, L. X. Wang, Z. Y. Lin, *Adv. Funct. Mater.* **2008**, *18*, 928; d) H. F. Chen, T. C. Wang, S. W. Lin, W. Y. Hung, H. C. Dai, H. C. Chiu, K. T. Wong, M. H. Ho, T. Y. Cho, C. W. Chen, C. C. Lee, *J. Mater. Chem.* **2012**, *22*, 15620; e) F. Lindla, M. Boesing, C. Zimmermann, F. Jessen, P. van Gemmern, D. Bertram, D. Keiper, N. Meyer, M. Heuken, H. Kalisch, R. H. Jansen, *Appl. Phys. Lett.* **2009**, *95*, 213305.

[5] a) M. A. Baldo, D. F. O'Brien, Y. You, A. Shoustikov, S. Sibley, M. E. Thompson, S. R. Forrest, *Nature* **1998**, *395*, 151; b) Y. Kawamura, K. Goushi, J. Brooks, J. J. Brown, H. Sasabe, C. Adachi, *Appl. Phys. Lett.* **2005**, *86*, 071104; c) C. Adachi, M. A. Baldo, M. E. Thompson, S. R. Forrest, *J. Appl. Phys.* **2001**, *90*, 5048; d) V. Cleave, G. Yahioglu, P. Le Barny, R. H. Friend, N. Tessler, *Adv. Mater.* **1999**, *11*, 285.

[6] a) L. X. Xiao, Z. J. Chen, B. Qu, J. X. Luo, S. Kong, Q. H. Gong, J. J. Kido, *Adv. Mater.* **2011**, *23*, 926; b) C. Ulbricht, B. Beyer, C. Friebe, A. Winter, U. S. Schubert, *Adv. Mater.* **2009**, *21*, 4418; c) Z. Q. Chen, Z. Q. Bian, C. H. Huang, *Adv. Mater.* **2010**, *22*, 1534.

[7] a) S. Lamansky, P. Djurovich, D. Murphy, F. Abdel-Razzaq, H. E. Lee, C. Adachi, P. E. Burrows, S. R. Forrest, M. E. Thompson, *J. Am. Chem. Soc.* **2001**, *123*, 4304; b) A. Tsuboyama, H. Iwawaki, M. Furugori, T. Mukaide, J. Kamatani, S. Igawa, T. Moriyama, S. Miura, T. Takiguchi, S. Okada, M. Hoshino, K. Ueno, *J. Am. Chem. Soc.* **2003**, *125*, 12971; c) B. X. Mi, P. F. Wang, Z. Q. Gao, C. S. Lee, S. T. Lee, H. L. Hong, X. M. Chen, M. S. Wong, P. F. Xia, K. W. Cheah, C. H. Chen, W. Huang, *Adv. Mater.* **2009**, *21*, 339; d) G. J. Zhou, C. L. Ho, W. Y. Wong, Q. Wang, D. G. Ma, L. X. Wang, Z. Y. Lin, T. B. Marder, A. Beeby, *Adv. Funct. Mater.* **2008**, *18*, 499; e)R. J. Wang, L. J. Deng, T. Zhang, J. Y. Li, *Dalton Trans.* **2012**, *41*, 6833.

[8] a) L. S. Hung, C. H. Chen, *Mat. Sci. Eng. R* **2002**, *39*, 143; b) V. V. Grushin, N. Herron, D. D. LeCloux, W. J. Marshall, V. A. Petrov, Y. Wang, *Chem. Commun.* **2001**, 1494; c) Z. A. Bao, A. J. Lovinger, J. Brown, *J. Am. Chem. Soc.* **1998**, *120*, 207; d) Y. Wang, N. Herron, V. V. Grushin, D. LeCloux, V. Petrov, *Appl. Phys. Lett.* **2001**, *79*, 449.

[9] C. L. Chin, W. C. Chen, K. L. Cheng, US Patent 7,799,918, **2010**.

[10] K. A. King, P. J. Spellane, R. J. Watts, *J. Am. Chem. Soc.* **1985**, *107*, 1431.

[11] Y. Kuwabara, H. Ogawa, H. Inada, N. Noma, Y. Shirota, *Adv. Mater.* **1994**, *6*, 677.

[12] a) G. Liaptsis, K. Meerholz, *Adv. Funct. Mater.* **2013**, *23*, 359; b) Y. H. Niu, M. S. Liu, J. W. Ka, J. Bardeker, M. T. Zin, R. Schofield, Y. Chi, A. K. Y. Jen, *Adv. Mater.* **2007**, *19*, 300; c) C. Y. Lin, Y. C. Lin, W. Y. Hung, K. T. Wong, R. C. Kwong, S. C. Xia, Y. H. Chen, C. I. Wu, *J. Mater. Chem.* **2009**, *19*, 3618.

[13] a) S. M. Park, Y. H. Kim, Y. Yi, H. Y. Oh, J. W. Kim, *Appl. Phys. Lett.* **2010**, *97*, 063308; b) W. S. Jeon, J. S. Park, L. Li, D. C. Lim, Y. H. Son, M. C. Suh, J. H. Kwon, *Org. Electron.* **2012**, *13*, 939.

[14] J. H. Jou, C. C. Chen, W. B. Wang, M. F. Hsu, C. J. Wang, C. T. Chen, M. F. Wu, H. Y. Chen, J. J. Shyue, C. L. Chin, *Org. Light Emitting Mater. Devices XII* **2008**, 7051.